Robust Type-II Weyl Semimetal Phase in Transition Metal Diphosphides XP_2 (X = Mo, W)

G. Autès,[1,2] D. Gresch,[3] M. Troyer,[3] A. A. Soluyanov,[3,4] and O. V. Yazyev[1,2]
[1]Institute of Physics, Ecole Polytechnique Fédérale de Lausanne (EPFL), CH-1015 Lausanne, Switzerland
[2]National Centre for Computational Design and Discovery of Novel Materials MARVEL, Ecole Polytechnique Fédérale de Lausanne (EPFL), CH-1015 Lausanne, Switzerland
[3]Theoretical Physics and Station Q Zurich, ETH Zurich, 8093 Zurich, Switzerland
[4]Department of Physics, St. Petersburg State University, St. Petersburg 199034, Russia
(Received 29 February 2016; revised manuscript received 21 June 2016; published 1 August 2016)

The recently discovered type-II Weyl points appear at the boundary between electron and hole pockets. Type-II Weyl semimetals that host such points are predicted to exhibit a new type of chiral anomaly and possess thermodynamic properties very different from their type-I counterparts. In this Letter, we describe the prediction of a type-II Weyl semimetal phase in the transition metal diphosphides MoP_2 and WP_2. These materials are characterized by relatively simple band structures with four pairs of type-II Weyl points. Neighboring Weyl points have the same chirality, which makes the predicted topological phase robust with respect to small perturbations of the crystalline lattice. In addition, this peculiar arrangement of the Weyl points results in long topological Fermi arcs, thus making them readily accessible in angle-resolved photoemission spectroscopy.

DOI: 10.1103/PhysRevLett.117.066402

Topological semimetals host band degeneracies in the vicinity of the Fermi level E_F that are associated with certain integer-valued topological invariants [1–9]. Since these invariants cannot continuously change their values, the associated degeneracies are protected against perturbations. One such semimetal phase—the Weyl semimetal (WSM)—hosts pointlike linear band crossings of two bands with linear dispersion, the so-called Weyl points (WPs), in the vicinity of E_F. These WPs represent sources or sinks of Berry curvature, and their associated topological invariant is the Chern number $\mathcal{C} = \pm 1$ computed on a surface in momentum space that encloses the WP. Positive (negative) Chern numbers correspond to a source (sink) of the Berry curvature. A variety of topology-driven physical phenomena is predicted and observed in WSMs, ranging from the observation of open Fermi arcs in the surface spectrum [2,10] to the realization of the chiral anomaly of quantum field theory [11–17].

It was recently shown [18] that unlike standard Lorentz-invariant field theory, condensed matter physics has two distinct types of Weyl fermions, and hence WSMs. While standard type-I Weyl fermions with closed Fermi surfaces were discovered in materials of the TaAs family [8,9,19–25], the novel type-II Weyl fermions appear at the boundary between electron and hole pockets, leaving an open Fermi surface that results in the anisotropic chiral anomaly [18,26]. Two representatives of type-II WSMs materials considered to date are the orthorhombic low-temperature phases of WTe_2 and $MoTe_2$ [18,27–29]. Eight (four) type-II WPs appear in WTe_2 ($MoTe_2$) formed by the valence and conduction bands. In WTe_2 some of the carrier pockets become topologically nontrivial, while in $MoTe_2$ they are all trivial, and the two materials represent very different Fermi arc arrangements [18,28]. In both cases, however, the band structure is very complicated and the arrangement of WPs is sensitive to small changes in the crystal structure, which, in turn, is sensitive to temperature [27,28]. Moreover, the proximity of WPs with opposite Chern numbers in k space, the energy of the WPs above the Fermi level, as well as the existence of crossings between bands other than the topmost valence and the lowest conduction, at energies close to that of the WPs, make the experimental confirmation of the type-II Weyl phase in WTe_2 and $MoTe_2$ a challenging task. The identification of materials with stable and easily observable type-II WPs thus sets an important problem in the study of this new topological phase.

In this Letter, we predict the existence of the type-II WSM phase in the previously synthesized compounds MoP_2 and WP_2 [30,31]. The crystal structure of these compounds is different from the previously reported ditellurides, resulting in a simpler band structure around E_F and a qualitatively different arrangement of WPs located below the Fermi level with nearest nodes characterized by the same Chern numbers, thus being stable against annihilating each other upon small lattice perturbations. This stability results in the presence of robust clearly visible long Fermi arcs at the surfaces of these compounds, which we expect to be readily observable in angle-resolved photoemission spectroscopy (ARPES) experiments. Moreover, since the WPs are located well below the Fermi level, the origin of the arcs, at the touching

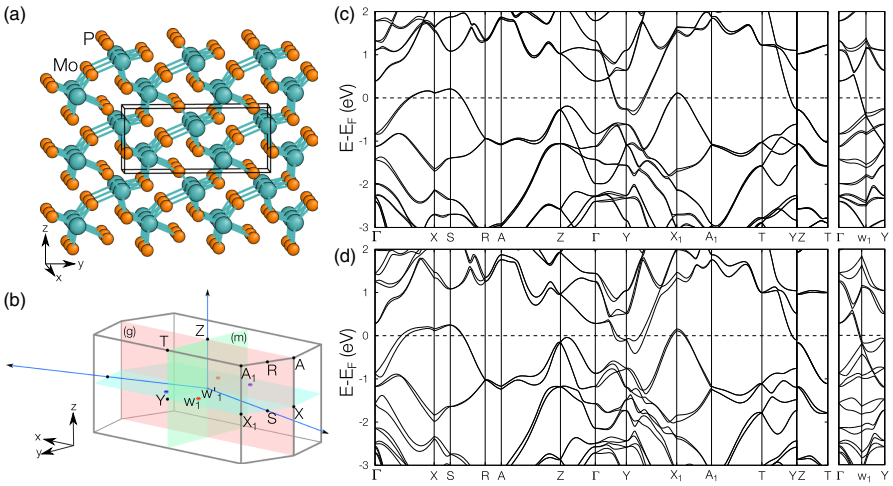

FIG. 1. (a) Crystal structure of MoP_2. The black box corresponds to the orthorhombic conventional unit cell. (b) Brillouin zone of MoP_2 showing the positions of Weyl nodes with positive (red) and negative (blue) Chern numbers. Band structures of (c) MoP_2 and (d) WP_2 plotted along high symmetry directions, as well as along the $\Gamma w_1 Y$ path in order to reveal the band crossings.

points of electron and hole pockets, is within the reach of ARPES experiments.

The two compounds were identified by performing a high-throughput screening of the band structure topology of materials in the inorganic crystal structure database (ICSD) [32], using the hybrid Wannier charge center technique [33,34] as implemented in the Z2Pack package [35]. Both MoP_2 and WP_2 crystallize in an orthorhombic base-centered structure [30,31] containing two formula units per unit cell as shown in Fig. 1(a). Both crystals are noncentrosymmetric and belong to the nonsymmorphic space group $Cmc2_1$ (36), which contains three symmetries: a C_2 screw axis along the [001] direction (2_1), a mirror plane normal to the [100] direction [m, shown in green in Fig. 1(b)], and a glide plane normal to the [010] direction [g, shown in red in Fig. 1(b)]. Although the crystalline symmetries of MoP_2 and WP_2 are similar to that of the ditellurides, the atomic structure of the phosphides is very different. While the structure of XTe_2 consists of van der Waals bonded layers, no layered structure exists in XP_2 materials.

The electronic structure of MoP_2 and WP_2 was computed from first principles [36,37]. The methodology is described in more detail in the Supplemental Material [38]. The band structures along the high-symmetry directions of the Brillouin zone (BZ) are shown in Figs. 1(c) and 1(d), for MoP_2 and WP_2, respectively. Both compounds share a similar semimetallic band structure, very different from that of the XTe_2 compounds, with an electron pocket around Y and a hole pocket in the vicinity of the XS direction. The Fermi contour of these pockets is shown with a dashed line in Fig. 2(a) for MoP_2 at $k_z = 0$. The main difference between the two compounds is that the spin-orbit coupling (SOC) is stronger in WP_2, which results in a larger band splitting compared to MoP_2.

The band structure of MoP_2 and WP_2 along the high symmetry lines of the BZ suggests that these compounds are ordinary semimetals. However, a more careful analysis reveals the presence of eight points in the $k_z = 0$ plane where the conduction and valence bands touch. This can be seen in Fig. 2(a), where we plot the energy difference between the lowest conduction and the highest valence bands in the $k_z = 0$ plane of the BZ. The gap closes at two inequivalent points w_1 and w_1', located away from any high-symmetry line. The positions of these points are listed in Table I. The six other points w_i and w_i' ($i = 2, 3, 4$) are related to w_1 and w_1' by mirror and time-reversal ($\mathcal{T}$) symmetries. In both compounds, w_1 and w_1' are at -0.410 and -0.364 eV relative to the Fermi level in MoP_2 and at -0.471 and -0.340 eV relative to the Fermi level in WP_2.

Analogously to the case of XTe_2, the existence of degeneracy points in the $k_z = 0$ plane of MoP_2 and WP_2 is due to the presence of the product symmetry $C_2\mathcal{T}$, which restricts a general 2×2 Hamiltonian in the plane to be of the form

$$\mathcal{H}(k_x, k_y, 0) = d_0(k_x, k_y)\sigma_0 + d_y(k_x, k_y)\sigma_y + d_z(k_x, k_y)\sigma_z, \quad (1)$$

where $\sigma_{y,z}$ are the corresponding Pauli matrices and σ_0 is the 2×2 unit matrix associated with the kinetic energy term of the type-II Weyl Hamiltonian [18]. The full derivation of the model Hamiltonian is presented in the Supplemental Material [38]. In order to establish that the degeneracies w_i and w_i' are indeed WPs, we computed the Chern numbers of surfaces enclosing these points following the method described in Ref. [18]. We find that both w_1 and w_1' carry a topological charge $\mathcal{C} = +1$ [38], while the charges of the other six points are obtained by symmetry arguments: mirror reflection flips the sign of the Chern number of a WP; thus, $w_{2,4}$ and $w_{2,4}{}'$ have $\mathcal{C} = -1$, while $\mathcal{T}$ reflection preserves it, so $\mathcal{C} = +1$ for w_3 and w_3'.

The WPs in MoP_2 and WP_2 are of type II as can be concluded by examining the Fermi surface at the energies of w_1 and w_1', shown in Fig. 2(b) for the case of MoP_2. Both nodes appear at the points of contact between the electron pocket located around Y and the hole pocket located along

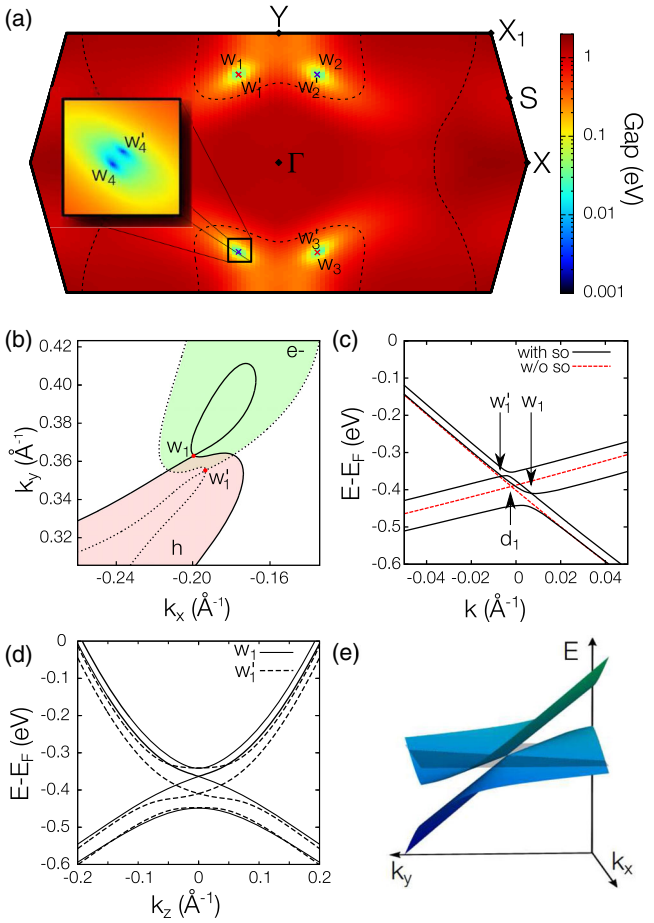

FIG. 2. (a) Energy difference between the lowest conduction band and the highest valence band of MoP_2 in the $k_z = 0$ plane of the Brillouin zone. The crosses correspond to the eight Weyl nodes with Chern numbers $\mathcal{C} = +1$ (red) and -1 (blue). The dashed lines show the contours of the hole and electron pockets at the Fermi level in the $k_z = 0$ plane. (b) Constant energy contour of the MoP_2 hole (red) and electron (green) pockets in the $k_z = 0$ plane at the energy of w_1 (continuous line) and of w_1' (dashed line). (c) Band structure of MoP_2 along the $w_1 w_1'$ line in the $k_z = 0$ plane with (black) and without (red) spin-orbit coupling. (d) Band structure of MoP_2 along k_z at k_x and k_y corresponding to the Weyl points w_1 (continuous line) and w_1' (dotted line). (e) Energy dispersion around the type-II Weyl point w_1 in the $k_z = 0$ plane.

the XS direction. To further confirm this conclusion, we fitted the *ab initio* band structure in the vicinity of the WPs to find the coefficients d_i of Eq. (1) to the linear order in $\mathbf{k}$ [38]. For both the w_1 and w_1' points, the kinetic term dominates the spectrum along the k_y direction around the WP, as illustrated in Fig. 2(e) for the WP w_1. The dominant kinetic term in the k_y direction suggests a possible observation of the type-II chiral anomaly [18] in XP_2 compounds when both electric and magnetic fields are applied along this direction.

The WPs w_1 and w_1' are separated in energy. To understand the origin of this separation, we note that the two

TABLE I. Positions, Chern numbers, and energies of the Weyl points in MoP_2 and WP_2.

		k_x (Å^{-1})	k_y (Å^{-1})	Chern number $\mathcal{C}$	$E - E_F$ (eV)
MoP_2	w_1	−0.2010	0.3627	+1	−0.410
MoP_2	w_1'	−0.1939	0.3516	+1	−0.364
WP_2	w_1	−0.2627	0.3165	+1	−0.471
WP_2	w_1'	−0.2577	0.2818	+1	−0.340

points are formed by spin-split bands, as can be concluded from Figs. 2(c) and 2(d), where the energy dispersion of MoP_2 is shown along a path connecting the two WPs in the $k_z = 0$ plane and along the k_z direction, respectively. Indeed, for a calculation performed without taking into account SOC, the electron and hole pockets touch at four crossing points d_i in the $k_z = 0$ plane, which have the associated topological charge $\mathcal{C} = \pm 2$ and correspond to the superposition of two WPs of the same chirality, as expected for SU(2) symmetry [39]. These double WPs are split by the SOC into single nodes w_i and w_i' [see Fig. 2(c)] that have the same chirality.

The magnitude of the splitting in energy and k space between the two adjacent WPs w_i and w_i' is hence directly related to the strength of the SOC. These splittings are larger in WP_2 (131 meV and 0.035 Å^{-1}) than in MoP_2 (46 meV and 0.013 Å^{-1}) (see Table I), as expected due to the larger SOC strength in W. This suggests the possibility of tuning the separation between the WPs in these compounds in both energy and momentum by applying strain or chemical substitution, since this changes the effective SOC.

Unlike the case of ditellurides, the neighboring WPs in XP_2 materials have the same chirality, and thus cannot annihilate each other. This implies that MoP_2 and WP_2 realize a stable type-II WSM phase that is far from a possible topological phase transition caused by a merging of the opposite chirality WPs. Opposite chirality WPs can annihilate when they reach the same point of the 3D BZ, so the smallest distance in k space between WPs with opposite Chern number $\mathcal{C}$ can be considered as a measure of the stability of the WSM phase. We find this distance to be 0.38 Å^{-1} and 0.52 Å^{-1} in MoP_2 and WP_2, respectively, which constitutes 20% and 26% of the corresponding inverse lattice constants. These numbers can be compared to the distance between opposite chirality WPs in the TaAs materials family, in particular TaP where the distance is the longest [8] and is 0.09 Å^{-1} (4% of the inverse lattice constant). The distance between the neighboring opposite chirality WPs in XTe_2 is 0.7% of the inverse lattice constant. This robustness is confirmed by comparing the evolution of the band structure of MoP_2 and WTe_2 under isotropic strain. In WTe_2, the relative positions of the WPs are highly sensitive to the variation of the lattice constant, leading to the elimination of the WSM phase for strains

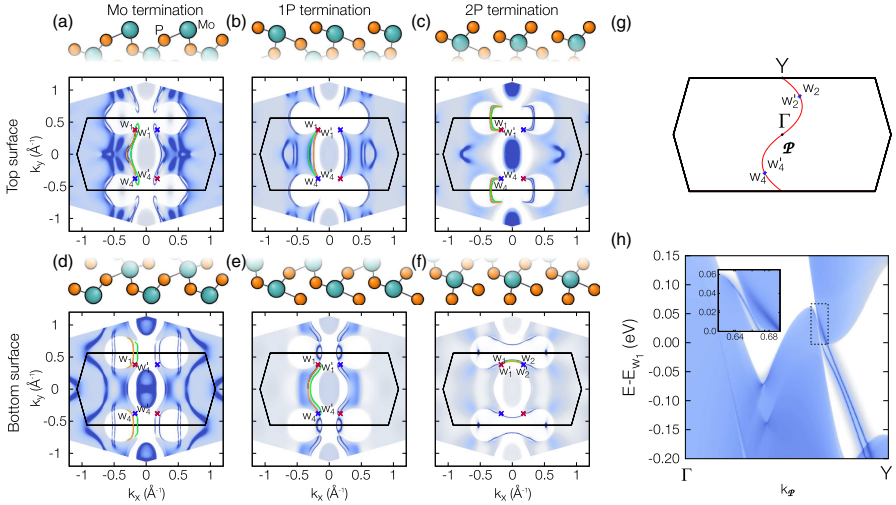

FIG. 3. Surface density of states of [(a),(b),(c)] the top and [(d),(e),(f)] the bottom (001) surfaces with Mo and P terminations 1P and 2P at the energy of the Weyl node w_1. The green and orange lines indicate the topological Fermi arcs connecting the w_i and w_i' WPs, respectively. (g) Cut in the $k_z = 0$ plane of the $\mathcal{T}$-symmetric plane $\mathcal{P}$ with $\mathbb{Z}_2$ invariant 1. (h) Surface density of states of the top P-terminated surface 2P along $\mathcal{P}$ from Γ to Y. The inset panel shows a magnified view of the region in the proximity of the hole and electron pockets. Only one of the two surface states is topological, connecting the electron and hole pockets.

$\varepsilon < -0.5\%$. In MoP_2, the WPs remain unaffected in a very broad range of strain [38].

One evident consequence of the large k-space separation of opposite chirality WPs in XP_2 is the possibility of the observation of extended topological Fermi arcs in the surface of these materials. For type-I WPs, which have a pointlike Fermi surface, these Fermi arcs connect the projections of the opposite chirality WPs onto the surface. In contrast, the Fermi surface of the type-II WPs is open and the projection of the points is generally hidden within the projection of a charge-carrier pocket.

We consider the (001) surface of MoP_2 and WP_2, since the eight WPs project onto distinct points of the corresponding surface BZ, allowing for the observation of Fermi arcs. We find that at all energies all electron and hole pockets enclose an equal number of chiral and antichiral WPs; therefore, the Chern number of all these pockets vanishes. From this perspective, no Fermi arcs connecting electron and hole pockets are expected. Indeed, at E_F we find that the projected WPs are covered by the projection of the electron pocket around the Y point and no Fermi arcs can be observed. However, we do find topological Fermi arcs in these materials at lower energies as we explain below.

We computed the surface density of states of MoP_2 using the tight-binding model, obtained from the bulk Wannier functions [40] for Mo d and P p orbitals, in order to compute the Green's function of the semi-inifnite surface according to the method introduced in Ref. [41]. Three possible surface terminations were investigated: one Mo terminated and two P terminated denoted as 1P and 2P. Furthermore, the top and bottom (001) surfaces of MoP_2 are inequivalent, thus giving rise to six different configurations [see Figs. 3(a)–3(f)]. The surface densities of states at the energy of w_1, 0.41 eV below E_F, all show two distinct Fermi arcs. One of these arcs connects two w_i points of opposite chirality [green line in Figs. 3(a)–3(f)], while the other one connects two w_i' points of opposite chirality [orange line in Figs. 3(a)–3(f)]. Both the connectivity and the shape of the Fermi arcs depend on the details of the surface termination. For the Mo and 1P top surfaces as well as for the 1P bottom surface, the Fermi arcs connect w_1 (w_1') and w_4 (w_4') within the surface BZ, which is shown as a black hexagon in Fig. 3. On the 2P top surface and the Mo bottom surface w_1 (w_1') is connected by a Fermi arc to w_4 (w_4') across the surface BZ boundary. Finally, on the 2P bottom surface, the Fermi arcs connect the w_1 (w_1') and w_2 (w_2') WPs.

While the connectivity of these Fermi arcs depends on a particular surface, one can argue that the arcs themselves are of topological origin. In order to demonstrate this we computed the $\mathbb{Z}_2$ invariant on the $\mathcal{T}$-symmetric plane $\mathcal{P}$ shown in Fig. 3(g) and find it to be nontrivial (see the Supplemental Material for details [38]). This implies that this cut of the BZ, on which the spectrum is gapped at all points, is a quantum spin Hall effect system [42], and therefore it is guaranteed to show topologically protected edge states. In other words, any line cut of the (001) surface BZ that passes between the two WPs has to cross a topological Fermi arc as shown in Fig. 3(h). The conclusion that the Fermi arcs connecting points w_i and w_i' are of topological origin agrees with the values of $\mathbb{Z}_2$ invariants defined on different $\mathcal{T}$-symmetric planes of the BZ, as further discussed in the Supplemental Material [38].

The predicted Fermi arcs span extended regions of k space and are localized below the Fermi level. Therefore, they should be readily observable in ARPES experiments on a cleaved (001) surface of XP_2 compounds. Experimental observation of these arcs, which originate and terminate at the touching points of electron and hole pockets, will provide an unambiguous evidence of the type-II Weyl fermions in these materials. It should be noted that other surface states are visible in Figs. 3(a)–3(f). A careful examination of the electronic structure shows that these states do not originate from Weyl points and are thus topologically trivial, as discussed in the Supplemental Material [38].

In conclusion, we theoretically identified a new family of type-II Weyl semimetals in the transition disphophides

MoP_2 and WP_2. The Brillouin zone of these materials contains four pairs of Weyl nodes with the same chirality in the $k_z = 0$ plane, which implies robustness of the predicted Weyl semimetal phase. We predict that a type-II chiral anomaly should be observable in these compounds and that long Fermi arcs should be detectable by ARPES experiments on the [001] surface with a great variety of possible arrangements depending on the surface termination.

G. A. and O. V. Y. acknowledge support by the NCCR Marvel and the ERC Starting grant "TopoMat" (Grant No. 306504). First-principles electronic structure calculations have been performed at the Swiss National Supercomputing Centre (CSCS) under Project No. s675. D. G., A. A. S., and M. T. were supported by Microsoft Research, the European Research Council through ERC Advanced Grant SIMCOFE, and the Swiss National Science Foundation through the National Competence Centers in Research MARVEL and QSIT.

[1] G. E. Volovik, *The Universe in a Helium Droplet* (Oxford University Press, New York, 2009).
[2] X. Wan, A. M. Turner, A. Vishwanath, and S. Y. Savrasov, Phys. Rev. B **83**, 205101 (2011).
[3] A. A. Burkov and L. Balents, Phys. Rev. Lett. **107**, 127205 (2011).
[4] Z. Wang, Y. Sun, X.-Q. Chen, C. Franchini, G. Xu, H. Weng, X. Dai, and Z. Fang, Phys. Rev. B **85**, 195320 (2012).
[5] S. M. Young, S. Zaheer, J. C. Y. Teo, C. L. Kane, E. J. Mele, and A. M. Rappe, Phys. Rev. Lett. **108**, 140405 (2012).
[6] Z. K. Liu *et al.*, Nat. Mater. **13**, 677 (2014).
[7] Z. K. Liu *et al.*, Science **343**, 864 (2014).
[8] H. Weng, C. Fang, Z. Fang, B. A. Bernevig, and X. Dai, Phys. Rev. X **5**, 011029 (2015).
[9] S.-M. Huang *et al.*, Nat. Commun. **6**, 7373 (2015).
[10] M. A. Silaev and G. E. Volovik, Phys. Rev. B **86**, 214511 (2012).
[11] H. Nielsen and M. Ninomiya, Phys. Lett. **130B**, 389 (1983).
[12] A. A. Zyuzin and A. A. Burkov, Phys. Rev. B **86**, 115133 (2012).
[13] P. Hosur and X. Qi, C.R. Phys. **14**, 857 (2013).
[14] G. E. Volovik, JETP Lett. **98**, 753 (2014).
[15] J. Xiong, S. K. Kushwaha, T. Liang, J. W. Krizan, W. Wang, R. J. Cava, and N. P. Ong, arXiv:1503.08179.
[16] C.-L. Zhang *et al.*, Nat. Commun. **7**, 10735 (2016).
[17] X. Huang, L. Zhao, Y. Long, P. Wang, D. Chen, Z. Yang, H. Liang, M. Xue, H. Weng, Z. Fang, X. Dai, and G. Chen, Phys. Rev. X **5**, 031023 (2015).
[18] A. A. Soluyanov, D. Gresch, Z. Wang, Q. Wu, M. Troyer, X. Dai, and B. A. Bernevig, Nature (London) **527**, 495 (2015).
[19] S.-Y. Xu *et al.*, Science **349**, 613 (2015).
[20] B. Q. Lv, H. M. Weng, B. B. Fu, X. P. Wang, H. Miao, J. Ma, P. Richard, X. C. Huang, L. X. Zhao, G. F. Chen, Z. Fang, X. Dai, T. Qian, and H. Ding, Phys. Rev. X **5**, 031013 (2015).
[21] B. Q. Lv *et al.*, Nat. Phys. **11**, 724 (2015).
[22] L. X. Yang *et al.*, Nat. Phys. **11**, 728 (2015).
[23] S.-Y. Xu *et al.*, Nat. Phys. **11**, 748 (2015).
[24] N. Xu *et al.*, Nat. Commun. **7**, 11006 (2016).
[25] S.-Y. Xu *et al.*, Sci. Adv. **1**, e1501092 (2015).
[26] G. Volovik and M. Zubkov, Nucl. Phys. **B881**, 514 (2014).
[27] Y. Sun, S.-C. Wu, M. N. Ali, C. Felser, and B. Yan, Phys. Rev. B **92**, 161107 (2015).
[28] Z. Wang *et al.*, arXiv:1511.07440.
[29] T.-R. Chang *et al.*, Nat. Commun. **7**, 10639 (2016).
[30] S. Rundqvist and T. Lundström, Acta Chem. Scand. **17**, 37 (1963).
[31] R. Rühl and W. Jeitschko, Monatshefte fur Chemie Chem. Mon. **114**, 817 (1983).
[32] G. Bergerhoff, R. Hundt, R. Sievers, and I. D. Brown, J. Chem. Inf. Model. **23**, 66 (1983).
[33] A. A. Soluyanov and D. Vanderbilt, Phys. Rev. B **83**, 235401 (2011).
[34] R. Yu, X. L. Qi, A. Bernevig, Z. Fang, and X. Dai, Phys. Rev. B **84**, 075119 (2011).
[35] D. Gresch, A. A. Soluyanov, G. Autès, O. V. Yazyev, B. A. Bernevig, D. Vanderbilt, and M. Troyer (to be published); package available at http://z2pack.ethz.ch/.
[36] P. Giannozzi *et al.*, J. Phys. Condens. Matter **21**, 395502 (2009).
[37] A. Dal Corso and A. Mosca Conte, Phys. Rev. B **71**, 115106 (2005).
[38] See Supplemental Material at http://link.aps.org/supplemental/10.1103/PhysRevLett.117.066402 for the details of the first-principles calculations, the derivation of the full model Hamiltonian, the computation of topological invariants, the effect of strain, and the description of the additional Weyl points present in the valence band.
[39] Z. J. Wang, A. A. Soluyanov, M. Troyer, X. Dai, and B. A. Bernevig (to be published).
[40] A. A. Mostofi, J. R. Yates, Y.-S. Lee, I. Souza, D. Vanderbilt, and N. Marzari, Comput. Phys. Commun. **178**, 685 (2008).
[41] A. Umerski, Phys. Rev. B **55**, 5266 (1997).
[42] C. L. Kane and E. J. Mele, Phys. Rev. Lett. **95**, 146802 (2005).